Wheel Torque Distribution Criteria for Electric Vehicles With Torque-Vectoring Differentials

Leonardo De Novellis, *Member, IEEE*, Aldo Sorniotti, *Member, IEEE*, and Patrick Gruber

***Abstract*—The continuous and precise modulation of the driving and braking torques of each wheel is considered the ultimate goal for controlling the performance of a vehicle in steady-state and transient conditions. To do so, dedicated torque-vectoring (TV) controllers that allow optimal wheel torque distribution under all possible driving conditions have to be developed. Commonly, vehicle TV controllers are based on a hierarchical approach, consisting of a high-level supervisory controller that evaluates a corrective yaw moment and a low-level controller that defines the individual wheel torque reference values. The problem of the optimal individual wheel torque distribution for a particular driving condition can be solved through an optimization-based control-allocation (CA) algorithm, which must rely on the appropriate selection of the objective function. With a newly developed offline optimization procedure, this paper assesses the performance of alternative objective functions for the optimal wheel torque distribution of a four-wheel-drive (4WD) fully electric vehicle. Results show that objective functions based on the minimum tire slip criterion provide better control performance than functions based on energy efficiency.**

***Index Terms*—Control allocation (CA), fully electric vehicle, optimization, torque-vectoring (TV) control.**

I. Introduction

FULLY ELECTRIC VEHICLES (FEVs) can have different topological layouts with in-wheel or onboard motor drives. This design flexibility, which is combined with the possibility of continuous modulation of the electric-motor torque, allows the implementation of advanced torque-vectoring (TV) control systems. In particular, based on the individual wheel torque control, novel TV strategies aimed at enhancing active safety [1]–[3] and "fun-to-drive" qualities [4] in all possible driving conditions can be developed. Indeed, by directly controlling the yaw moment through the actuation of electric drivetrains, a TV system extends the safe driving conditions to greater vehicle velocities during emergency transient maneuvers than a conventional vehicle dynamics control system based on the actuation of the friction brakes [5], [6]. Different electric vehicle layouts are currently analyzed for the demonstration of TV control strategies, including multiple individually controllable drivetrains [7]–[11] or one electric motor per axle coupled with an open mechanical differential or a TV mechanical differential, which is the solution discussed in this paper.

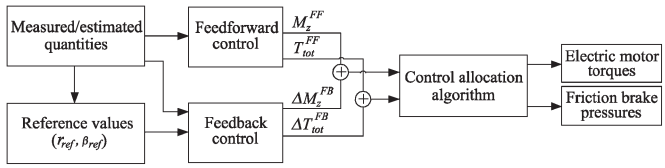

Fig. 1. Functional schematic of a typical TV controller for an FEV with multiple individually controllable drivetrains (also illustrated in [7] and [8]).

TV control structures are usually organized according to a hierarchical approach (see Fig. 1). A high-level vehicle dynamics controller generates a reference vehicle yaw rate, which is adopted by a feedback controller to compute the reference tractive/braking torque and yaw moment. The feedback controller is either based on sliding mode [12], [13], linear quadratic regulation [14], model predictive control [15], or robust control [16]. A feedforward contribution M_z^{FF}, e.g., based on maps, can be also included, as shown in Fig. 1, in such a way that the control yaw moment M_z^{TOT} is given by $M_z^{\mathrm{TOT}} = M_z^{\mathrm{FF}} + \Delta M_z^{\mathrm{FB}}$, where the feedback term ΔM_z^{FB} compensates the inaccuracies, the disturbances, or the variation of the vehicle parameters (such as vehicle mass, position of the center of gravity, etc.) considered for the derivation of the feedforward maps.

At a lower level, the objective of the control allocation (CA) is to generate appropriate commands for the actuators to produce the desired control action in terms of traction/braking torque and yaw moment. When the number of actuators is larger than the number of reference control actions, the CA problem can be solved by minimizing an assigned objective function. This is achieved with simplified formulas based on the vertical load distribution [17], [18] or with more advanced techniques, such as weighted pseudoinverse CA [10], [19], linear matrix inequality [20], or quadratic programming with inequality constraints [21]. The optimization algorithms most commonly employed for online CA schemes are active set, fixed point, and accelerated fixed point. The published methods are shown to be successful, but their application and analysis are limited as their tuning is carried out through the optimization of the vehicle performance during specific maneuvers [22] and not the full range of possible operating conditions. More importantly, the effect of the possible alternative formulations of the objective functions for CA on the overall performance is not explored in the literature.

Manuscript received February 28, 2013; revised July 6, 2013 and September 3, 2013; accepted October 22, 2013. Date of publication November 6, 2013; date of current version May 8, 2014. This work was supported in part by the European Union through the Seventh Framework Programme (FP7/2007–2013) under Grant 284708. The review of this paper was coordinated by Prof. M. Benbouzid.

The authors are with the Department of Mechanical Engineering Sciences, University of Surrey, Guildford GU2 7XH, U.K. (e-mail: l.denovellis@surrey.ac.uk; a.sorniotti@surrey.ac.uk; p.gruber@surrey.ac.uk).

Color versions of one or more of the figures in this paper are available online at http://ieeexplore.ieee.org.

Digital Object Identifier 10.1109/TVT.2013.2289371

TV control can have a major impact on the general driving experience. Most of the time, the driver operates the vehicle in steady-state or slowly varying conditions at lateral acceleration levels a_y below 0.5 g [23]. During these sub-limit conditions, the continuous yaw moment control can significantly improve the vehicle cornering response. As recently pointed out in [24]: "Despite the significant volume of theoretical studies of TV on vehicle handling control, there is no widely accepted design methodology of how to exploit it to improve vehicle handling and stability significantly." To address this issue, novel tools for the design of TV control systems have to be proposed and assessed. This paper presents a methodology based on the definition of a set of reference understeer characteristics and the comparison of different CA criteria.

Vehicle steady-state cornering response is usually assessed in terms of its understeer characteristic, which is expressed by the dynamic steering-wheel angle $\delta_{\rm dyn}$ ($\delta_{\rm dyn} = \delta - \delta_{\rm kin}$, where δ is the actual steering-wheel angle, and $\delta_{\rm kin}$ is the kinematic steering-wheel angle) as a function of a_y [25]. In general, in a passenger car, $\delta_{\rm dyn}(a_y)$ increases monotonically and nearly linearly up to a value of lateral acceleration $a_y^* \simeq 0.5$ g for high friction conditions. Correspondingly, the understeer gradient $K_U = \partial\delta_{\rm dyn}/\partial a_y$ of the vehicle is nearly constant. Beyond this linear region, $\delta_{\rm dyn}(a_y)$ is nonlinear and tends to an asymptotic value corresponding to $a_{y,\,\max}$ when the tire friction limits are reached. In contrast to vehicles without TV control, where the specific understeer characteristics are determined by the tire properties, geometrical and inertial parameters, and the suspension elastokinematics [26], [27], the understeer characteristics of a vehicle equipped with a TV system can be designed to achieve almost any desired behavior. For example, the understeer gradient K_U in the linear part of the characteristic could be imposed. Moreover, the width of the linear portion of $\delta_{\rm dyn}(a_y)$ (indicated by a_y^*) could be increased, or the maximum lateral acceleration $a_{y,\,\max}$ could be altered, with the constraints dictated by tire friction limits [28].

In addition to the advantages during pure cornering maneuvers, continuous TV control has the potential to improve the handling response of a vehicle while braking or accelerating. As will be discussed in Section II, the understeer characteristic of a vehicle (without TV) varies markedly with different levels of longitudinal acceleration a_x. Despite the significant influence of accelerating and braking, the understeer characteristics for nonzero a_x are normally not considered and analyzed. This restriction mainly results from limitations imposed by the typical vehicle dynamics simulation techniques or testing procedures used to derive the zero a_x cornering response plots, namely, skidpad tests or ramp-steer maneuvers.

This paper deals with the detailed analysis of different approaches for the optimal wheel torque distribution for vehicle TV control. In particular, the following three points are presented and discussed.

1) An experimentally validated vehicle model based on a quasi-static approach is introduced, to derive the vehicle understeer characteristics in conditions of nonzero a_x values. The model can be also used to estimate the transient vehicle response through moment-method-based techniques [29].

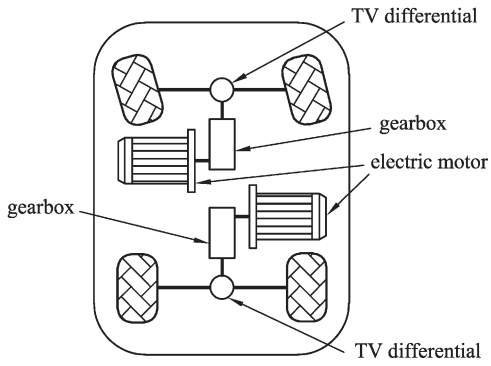

Fig. 2. Functional schematic of the case-study 4WD electric vehicle layout comprising one onboard electric motor and one TV differential on each axle.

TABLE I
MAIN ELECTRIC VEHICLE PARAMETERS

Symbol	Description	Quantity
m	Overall vehicle mass	1940 kg
x_F	Distance from the center of gravity to the front axle	1 m
x_R	Distance from the center of gravity to the rear axle	1.6 m
$2y_{F/R}$	Front and rear track width	1.625 m
h_{CG}	Height of the vehicle center of mass	0.66 m
-	Tires	235/55 R19
$P_{M,MAX}$	Maximum electric motor power	228 kW
$n_{M,MAX}$	Maximum electric motor speed	14000 RPM
τ_1	First stage transmission gear ratio	3.33
τ_2	Second stage transmission gear ratio	3

2) A novel offline optimization design procedure, which is based on the quasi-static model, is presented. The procedure generates the maps of the feedforward contribution of the reference yaw moment and of the CA actuation to achieve a set of reference understeer characteristics, including the compensation (or partial compensation) of their spread as a function of a_x.
3) The performances of different CA objective functions are contrasted, and the results and sensitivity to the electric-motor drive parameters are discussed. This is achieved through the aforementioned offline procedure, which allows the *a priori* analysis of the results, independently from specific maneuvers in the time domain.

II. VEHICLE MODELING

The case-study vehicle (see Fig. 2 and Table I) is a four-wheel-drive (4WD) sport utility vehicle (SUV) equipped with one switched reluctance motor per axle, which is connected to the wheels through a single-speed transmission, a TV differential, and two half-shafts with constant velocity joints.

This FEV topology combines the advantages of an individually controlled 4WD layout, with the lower cost associated with two electric-motor drives instead of four. The TV differentials of the specific FEV permit left/right TV within each axle with a maximum torque bias of 1000 Nm, whereas the two central motors provide front/rear torque distribution, with the added benefit of a relatively simple management of fail-safe-related issues [18].

A. Model Description

A quasi-static vehicle model (according to the definition in [30]) was developed, assuming that the time derivatives of the main state variables of the system (vehicle sideslip angle β, roll angle φ, and tire longitudinal slip σ_i) are zero, as shown in the following:

$$\dot{\beta} = \dot{\varphi} = \dot{\sigma}_i = 0. \tag{1}$$

With this approach, the understeer characteristics for assigned values of a_x, the energy efficiency, and the moment method plots [31] can be quickly computed, avoiding the computationally demanding forward time integration of the equations of motion.

The quasi-static model [4] considers four degrees of freedom for modeling the chassis response (longitudinal, lateral, roll, and yaw motions). The equations of motion for each degree of freedom are written according to the sign conventions of the ISO standard [32], i.e.,

$$\sum_{i=1}^{4} F_{x_i} \cos\delta_{w_i} + \sum_{i=1}^{4} F_{y_i} \sin\delta_{w_i} - F_{\text{drag}} = m(\dot{u} - rv\beta) \tag{2}$$

$$\sum_{i=1}^{4} F_{x_i} \sin\delta_{w_i} + \sum_{i=1}^{4} F_{y_i} \cos\delta_{w_i} = m(\dot{u}\beta + ur) \tag{3}$$

$$\begin{aligned} &m(\dot{u}\beta + ur)(h_{\text{CG}} - d_{\text{CG}})\cos\varphi + mg(h_{\text{CG}} - d_{\text{CG}})\sin\varphi \\ &\quad - \left(\sum_{i=1}^{2} F_{x_{i_F}} \sin\delta_{w_{i_F}} + \sum_{i=1}^{2} F_{y_{i_F}} \cos\delta_{w_{i_F}}\right)(d_F - d_{\text{CG}}) \\ &\quad - \left(\sum_{i=1}^{2} F_{x_{i_R}} \sin\delta_{w_{i_R}} + \sum_{i=1}^{2} F_{y_{i_R}} \cos\delta_{w_{i_R}}\right)(d_R - d_{\text{CG}}) \\ &\quad = M_{\varphi_F} + M_{\varphi_R} \end{aligned} \tag{4}$$

$$\begin{aligned} M_z = &\sum_{i=1}^{4} F_{x_i} \cos\delta_{w_i} y_i + \sum_{i=1}^{4} F_{x_i} \sin\delta_{w_i} x_i + \sum_{i=1}^{4} F_{y_i} \cos\delta_{w_i} x_i \\ &+ \sum_{i=1}^{4} F_{y_i} \sin\delta_{w_i} y_i + \sum_{i=1}^{4} M_{z_i}. \end{aligned} \tag{5}$$

Subscripts "F" and "R" indicate the front and rear axles. M_z is the yaw moment required to maintain the vehicle in equilibrium conditions, consistently with the quasi-static approach. u is the longitudinal component of vehicle velocity v with respect to the vehicle reference system. x_i and y_i are the longitudinal and lateral distances between each tire and h_{CG} is the height of the vehicle center of gravity. d_{CG}, d_F, and d_R are the heights of the roll axis, which are evaluated at the vehicle center of gravity, the front suspension, and the rear suspension, respectively. The front and rear suspension antiroll moments, i.e., M_{φ_F} and M_{φ_R}, respectively, are computed through nonlinear lookup tables based on the respective roll stiffness values. F_{drag} is the aerodynamic drag force.

The longitudinal force F_{x_i}, the lateral force F_{y_i}, and the self-aligning moment M_{z_i} of the ith tire in its reference system are calculated by employing the Magic Formula model [23] as functions of the longitudinal slip σ_i, slip angle α_i, camber angle, tire–road friction coefficient, and vertical load F_{z_i}, which is expressed as

$$\begin{aligned} F_{z_i} = &F_{z0_i} + \varepsilon_1 \left(F_{\text{drag}} + m(\dot{u} - rv\beta)\right) \frac{h_{\text{CG}}}{2L} \\ &+ \varepsilon_2 \frac{\sum_{j=1}^{2} F_{x_{j_{F/R}}} \sin\delta_{w_{j_{F/R}}} + \sum_{j=1}^{2} F_{y_{j_{F/R}}} \cos\delta_{w_{j_{F/R}}}}{\sum_{j=1}^{2} |y_{j_{F/R}}|} \\ &\times d_{F/R} + \varepsilon_2 \frac{M_{\varphi_{F/R}}}{\sum_{j=1}^{2} |y_{j_{F/R}}|} \end{aligned} \tag{6}$$

where summations Σ_j are applied to the two wheels of the same axle, F_{z0_i} is the tire static vertical load, L is the vehicle wheelbase, $\varepsilon_1 = \pm 1$ depending on the axle, and $\varepsilon_2 = \pm 1$ depending whether the wheels are on the right side or the left side of the vehicle.

For the simulation of the drivetrain layout of the case-study vehicle (see Fig. 2), the model of an overdriven TV differential has been included (see [33] for the detailed analytical description). The wheel torque values are functions of the motor torque values and the differential clutch control torque values $T_{C_{\text{Left},\,F/R}}$ and $T_{C_{\text{Right},\,F/R}}$, which allow a torque bias between the two wheels of the same axle.

The electric-motor drives are modeled with experimentally derived electric power-loss maps that are functions of the primary operating variables, i.e., the torque, the speed, the input voltage, and the operating temperature. A realistic model of the vehicle battery and its losses based on the approach outlined in [34] has been implemented.

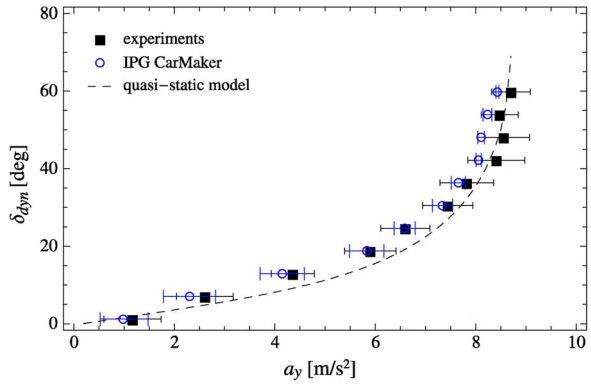

Fig. 3. Understeer characteristic of a front-wheel-drive SUV (without TV system) derived from skidpad tests, the quasi-static model, and the IPG CarMaker simulations. The horizontal bars shown for the tests in the time domain indicate the range of variation (in terms of the standard deviation with respect to the mean value) of a_y due to the steering-wheel angle oscillations that were measured during the maneuvers.

B. Model Validation

The understeer and sideslip characteristics of the quasi-static model were validated against experimental results obtained at the Lommel proving ground (Belgium) with an internal combustion engine driven SUV (see Fig. 3). The tire vertical, longitudinal, and lateral force characteristics and the sprung mass roll response, not measured directly in the experimental tests, were compared with the results provided by a vehicle

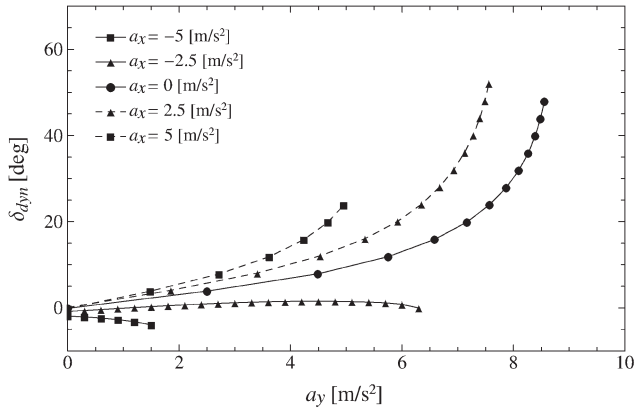

Fig. 4. Understeer characteristics of the case-study vehicle, without a TV control system, evaluated at $v = 90$ km/h and different values of a_x, ranging from -5 to 5 m/s^2 in steps of 2.5 m/s^2.

model created with CarMaker (IPG Automotive, Karlsruhe, Germany). The CarMaker model itself has been experimentally validated in steady-state and transient conditions.

C. Model Results and Discussion

Fig. 4 plots $\delta_{\rm dyn}$ as a function of a_y for a range of longitudinal accelerations a_x. The results are obtained with the quasi-static model of the 4WD case-study vehicle in conditions of absence of torque transfer on the TV differentials. In the solution of the equations of the quasi-static model, the same torque is imposed in traction on the front and rear axles. During braking, a 75:25 front-to-rear torque distribution is considered.

As shown in Fig. 4, a_x has a significant influence on K_U, even when $a_y = 0$. For instance, K_U ranges from -4.9 deg/g at $a_x = -5$ m/s^2 to $+27.3$ deg/g at $a_x = 5$ m/s^2. Moreover, the maximum achievable $\delta_{\rm dyn}$ reduces when $K_U < 0$.

The considerable change of the understeer gradient with a_x can be perceived by the driver as an "inconsistent" vehicle behavior already in normal driving conditions. To make the vehicle behave more predictably, a TV system can be used to (at least partially) compensate the variation of K_U. An approach for a qualitative limitation of the spread of the characteristics in Fig. 4 has been proposed in [31]. However, the presented TV algorithm is not based on a reference understeer characteristic and thus cannot provide an *a priori* definable amount of reduction of the spread of the understeer characteristics. Moreover, the TV controller cannot be used to achieve a desired understeer characteristic, for example, by modifying the K_U or the linear region according to target values. These issues are addressed by the procedure described in Section III.

III. Offline Optimization Procedure for the Design of the Understeer Characteristic

A. Procedure Description

An offline optimization procedure has been developed to generate the map for the feedforward component $M_z^{\rm FF}$ of the TV controller (see Fig. 1) for tracking a target understeer characteristic. At the same time, the procedure allows the offline evaluation of the distribution of motor torque, differential clutch torque, and friction brake pressures. These can be expressed as functions of the total reference wheel torque $(T_{\rm TOT})$ and $M_z^{\rm TOT}$, or as direct functions of five inputs: 1) the actual steering-wheel angle; 2) vehicle velocity; 3) the driver torque demand defined by the accelerator pedal position; 4) the position of the brake pedal, which is measured by the displacement sensor located in the pedal unit of the brake-by-wire system; and 5) the tire–road friction coefficient. For actual implementation of the TV controller, online estimation of the tire parameters, including tire–road friction coefficient μ, is required.

The offline procedure is designed to compare different cost functions for CA without the problems related to their implementation within an online CA algorithm (e.g., such as the approximated evaluation of the tire friction ellipse). In fact, online CA implies heavy numerical approximations, which depend on the analyzed objective function. Moreover, most of the CA algorithms are suitable only for quadratic formulations of the optimization problem. These reasons prevent the objective assessment of alternative CA criteria. Hence, a fair comparison of objective function formulations for CA can be carried out only through an offline procedure, missing at the moment in the literature [7]–[9].

The offline procedure consists of three steps (see Fig. 5).

Step 1: Definition of a set of reference understeer characteristics $\delta_{\rm dyn}(a_y, a_x)$. The following expression based on three parameters (i.e., $K_U(a_x)$, $a_y^*(a_x)$, and $a_{y,\max}(a_x)$) is proposed:

$$\begin{cases} a_y = \frac{1}{K_U}\delta_{\rm dyn}, & \text{if } \delta_{\rm dyn} < a_y^* K_U \\ a_y = a_{y,\max} + \left(a_y^* - a_{y,\max}\right) & \\ \qquad \times\ e^{\frac{a_y^* K_U - \delta_{\rm dyn}}{\left(a_{y,\max} - a_y^*\right) K_U}}, & \text{if } \delta_{\rm dyn} \geq a_y^* K_U. \end{cases} \tag{7}$$

Reference set $\delta_{\rm dyn}(a_y, a_x)$ constitutes one of the equality constraints in the optimization procedure.

Step 2: Definition of a set of equality and inequality constraints. The equality constraints are represented by the equations of the quasi-static model in Section II-A. The inequalities relate to limitations arising from the installed hardware components, such as: 1) electric-motor torque limitation, as a function of the electric-motor voltage, speed, and temperature; 2) battery power limitation, as a function of the battery state of charge, current, and temperature; 3) limitation of the TV differential actuation; 4) longitudinal slips σ_i, from the viewpoint of the limitation of their absolute values and/or their distribution between the four wheels; and 5) braking strategy and maximum friction braking torque.

Step 3: Optimization through minimization of an objective function. For instance, the following objective function J_P, which is based on an energy efficiency criterion, i.e., the minimization of the input power to the front and rear electric drivetrains ($P_{\ln_F}$ and $P_{\ln_R}$, respectively), is used:

$$J_P = P_{\ln_F} + P_{\ln_R}. \tag{8}$$

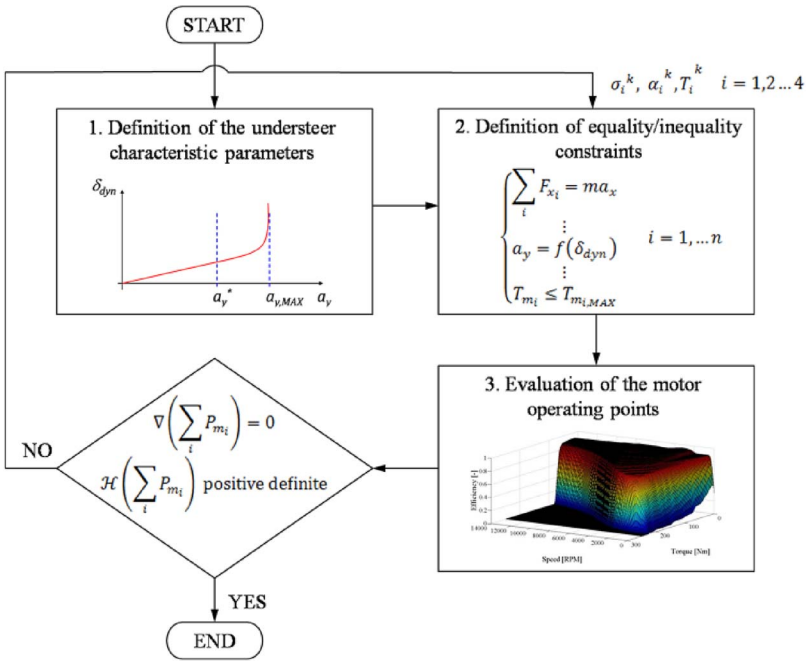

Fig. 5. Flowchart of the offline optimization procedure for the computation of the wheel torque distribution (in the figure, the objective function is based on the overall motor input power). For each iteration step, local minima are detected through the variation of the assigned initial conditions during the optimization loops for the same vehicle operating condition.

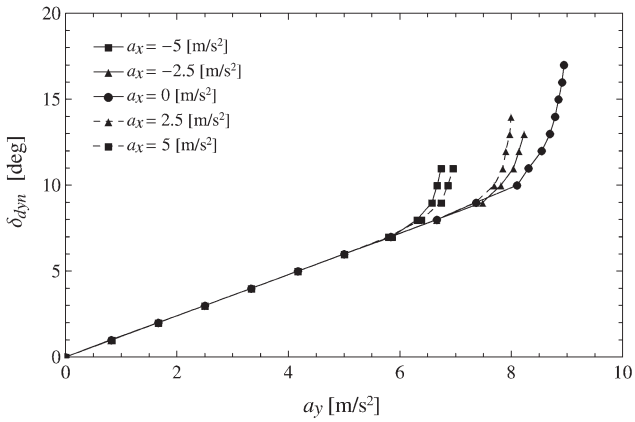

Fig. 6. Set of $\delta_{\mathrm{dyn}}(a_y, a_x)$ for the vehicle with TV at $v = 90$ km/h and values of a_x ranging from -5 to 5 m/s^2 in steps of 2.5 m/s^2, with $K_U = 12$ deg/g for all the characteristics.

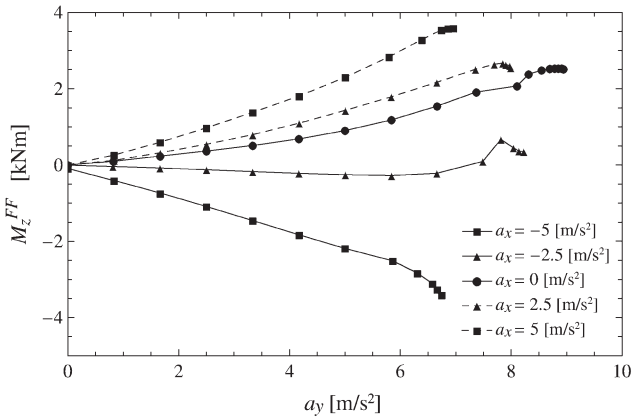

Fig. 7. Reference set of $M_z^{\mathrm{FF}}(a_y)$ for the vehicle with TV at $v = 90$ km/h and different values of a_x, ranging from -5 to 5 m/s^2 in steps of 2.5 m/s^2.

Due to the irregularities and local minima of the efficiency maps of the electric-motor drives, a suitable optimization algorithm was determined with an initial comparison of the performance of several routines (active set, sequential quadratic programming, trust-region reflective, and interior point). This was achieved by running the procedure with different initial conditions and then checking the outputs of the alternative algorithms. The selected formulation is the interior point method [35].

Fig. 6 plots one possible set of results for the understeer characteristics obtained with the optimization procedure for the case-study vehicle with TV control. Compared with Fig. 4, the understeer gradient in the linear region is constant and independent of the longitudinal acceleration. Therefore, the vehicle will show consistent and predictable cornering response. To obtain a more responsive vehicle, the understeer gradient in conditions of constant velocity for the controlled vehicle was selected to be lower than for the vehicle without TV. Despite the increased responsiveness in traction, the stability in braking is enhanced. Fig. 7 plots the corresponding set of $M_z^{\mathrm{FF}}(a_y)$. In traction, M_z^{FF} is positive to increase the vehicle yaw rate, and in braking, M_z^{FF} is negative to stabilize the vehicle.

Fig. 8 is the graph of the five major power losses for the vehicle with the understeer characteristic in Fig. 6 at $a_x = 2.5$ m/s^2. The highest gradient as a function of a_y belongs to the power-loss contribution $P_{\mathrm{LOSS},\,\alpha}$ relating to tire sideslip (due to the lateral slip velocity $v_{s,\,y_i}$ of each tire in its reference system), which is defined by

$$P_{\mathrm{LOSS},\,\alpha} = \sum_{i=1}^{4} F_{y_i} v_{s,\,y_i}. \tag{9}$$

The power consumption associated with the tire lateral forces represents an essential contribution for the vehicle steering

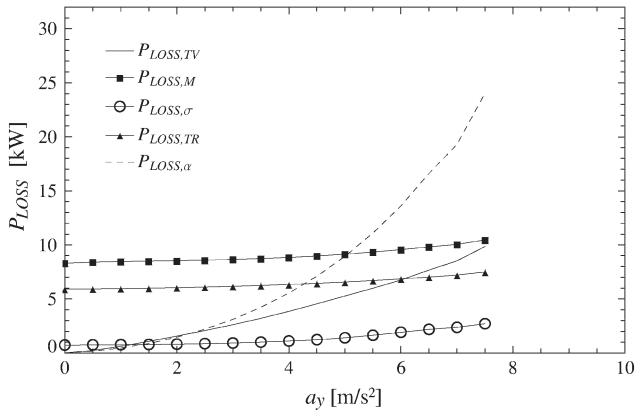

Fig. 8. Five major power-loss contributions evaluated for the vehicle with TV at $v = 90$ km/h and $a_x = 2.5$ m/s^2 for the understeer characteristic in Fig. 6.

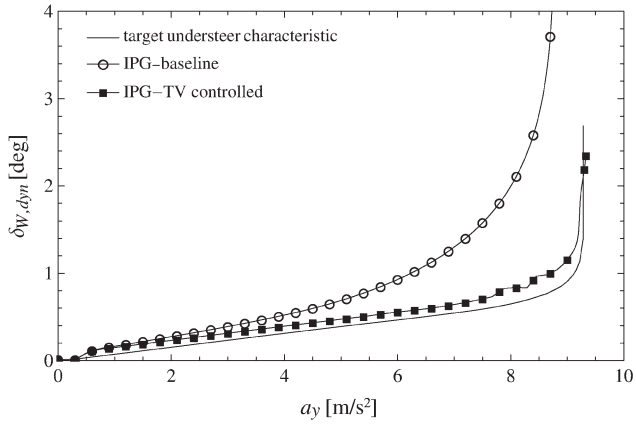

Fig. 9. Mean wheel steer angle $\delta_{w,dyn}(a_y)$ evaluated at $v = 90$ km/h. Comparison of the results for a ramp-steer maneuver obtained with the CarMaker–Simulink model of the baseline vehicle ("IPG-baseline"), the vehicle with TV control ("IPG-TV controlled"), and the quasi-static model. Parameters $K_U = 12$ deg/g, $a_y^* = 7$ m/s^2, and $a_{y,\max} = 9.3$ m/s^2 were considered in the optimization procedure.

capability; however, as shown in the following, this dissipative term can be minimized by a proper wheel torque distribution.

Moreover, the power losses due to the TV differentials $P_{\mathrm{LOSS,TV}} = P_{\mathrm{LOSS,TV}_F} + P_{\mathrm{LOSS,TV}_R}$ and the power losses arising from longitudinal tire slip $P_{\mathrm{LOSS},\sigma}$ (due to the longitudinal slip velocity v_{s,x_i} with respect to the reference system of each tire) increase markedly with a_y. $P_{\mathrm{LOSS},\sigma}$ and $P_{\mathrm{LOSS,TV}_{F/R}}$ are given by

$$P_{\mathrm{LOSS},\alpha} = \sum_{i=1}^{4} |F_{x_i} v_{s,x_i}| = \sum_{i=1}^{4} |F_{x_i} v_{x_i} \sigma_i| \quad (10)$$

$$P_{\mathrm{LOSS},TV_{F/R}} = |T_{C_{\mathrm{Left},F/R}} \Delta\omega_{C_{\mathrm{Left},F/R}}| + |T_{C_{\mathrm{Right},F/R}} \Delta\omega_{C_{\mathrm{Right},F/R}}| \quad (11)$$

where σ_i is the slip ratio of the tire, v_{x_i} is the velocity of the wheel center along the x-axis of the tire reference system, and $\Delta\omega_{C_{\mathrm{Left/Right},F/R}}$ are the slip speeds of the left and right clutches of the front and rear TV differentials.

In contrast, the power losses in the transmission $P_{\mathrm{LOSS,TR}}$ (excluding the TV differentials) and in the electric-motor drives $P_{\mathrm{LOSS,M}}$ (the largest contribution up to a value of $a_y \simeq 5$ m/s^2) marginally grow with a_y for the specific drivetrains. Similar behavior of the motor power losses has been evaluated under the same operating conditions for the vehicle without TV. As a consequence, the potential advantage of including the efficiency maps of the electric motor in the optimization procedure for CA is modest compared with the wheel-slip power-loss contribution.

B. Procedure Verification

To simulate the 4WD vehicle layout considered in this study, a vehicle model created in CarMaker by IPG Automotive has been connected to a dynamic model of two electric drivetrains, which is implemented in Matlab–Simulink. This model includes the first-order torsion dynamics and the plays of the drivetrain [36].

As means of verification of the optimization procedure, the created maps of the feedforward control action (to be applied to the motors and the differentials) were implemented in the CarMaker–Simulink model of the case-study FEV. For example, Fig. 9 compares the understeer characteristic of the baseline vehicle (without TV) simulated in CarMaker, i.e., the target understeer characteristic adopted within the optimization, and the understeer characteristic for the vehicle (in CarMaker) with only the feedforward TV control applied, during a ramp-steer maneuver in conditions of constant velocity. As shown in Fig. 9, the reference and actual characteristics match well already without the feedback controller. Moreover, as this good agreement was verified for several maneuvers (omitted here for brevity), we conclude that the feedback control would have only a marginal intervention within the overall controller in most conditions.

In addition, Fig. 9 highlights the benefits of the TV system in relation to K_U (15.7 deg/g for the baseline vehicle and 12 deg/g for the vehicle with TV), a_y^* (about 3.5 m/s^2 for the baseline vehicle and 7 m/s^2 for the vehicle with TV), and $a_{y,\max}$ (8.5 m/s^2 for the baseline vehicle and 9.3 m/s^2 for the vehicle with TV).

IV. Comparison of Alternative Objective Functions for Control Allocation

Based on results obtained with the offline optimization procedure, here, we evaluate and compare four alternative objective functions for CA in terms of their influence on vehicle steady-state performance. The investigated objective functions, which are outlined in [4] for a vehicle with individual motors at the wheels, are the following.

J_P, as introduced in (8), is the function based on the minimization of the overall input motor power.

J_{STD} is the function that minimizes the standard deviation of longitudinal tire slip with respect to the average slip of the four wheels, i.e.,

$$J_{\mathrm{STD}} = \sqrt{\sum_{i=1}^{4} \frac{\sigma_i^2}{4} - \left(\sum_{i=1}^{4} \frac{\sigma_i}{4}\right)^2}. \quad (12)$$

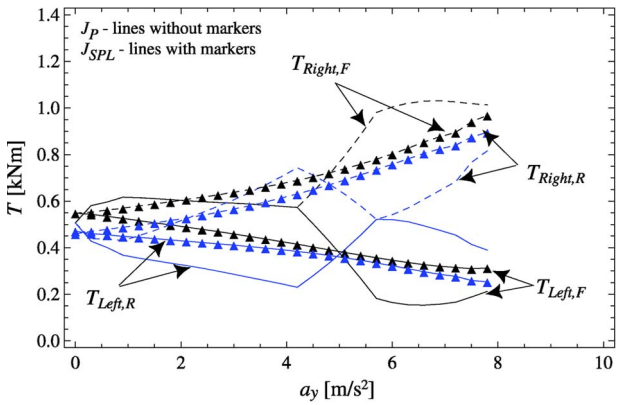

Fig. 10. Drivetrain torque values $T_{\mathrm{Right/Left},\,F/R}$ for the TV vehicle with the understeer characteristic in Fig. 6 at $v = 90$ km/h and $a_x = 2.5$ m/s^2 for J_P (lines without markers) and J_{SPL} (lines with markers).

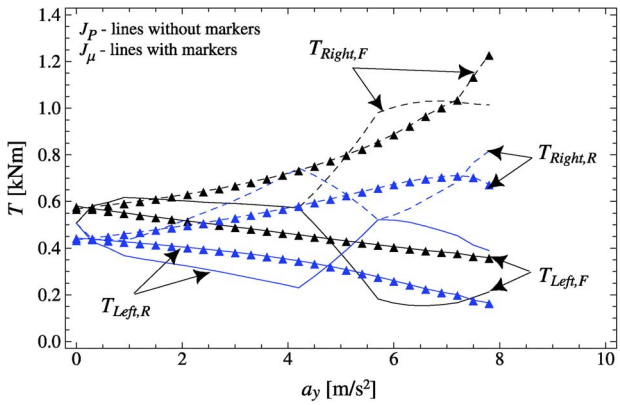

Fig. 11. Drivetrain torque values for the TV vehicle with the understeer characteristic in Fig. 6 at $v = 90$ km/h and $a_x = 2.5$ m/s^2 for J_P (lines without markers) and J_μ (lines with markers).

J_{SPL} is the function that minimizes the total longitudinal slip power loss, i.e.,

$$J_{\mathrm{SPL}} = \sum_{i=1}^{4} F_{x_i} v_{s,\,x_i}. \tag{13}$$

J_μ is the function that minimizes the average combined tire force coefficient, i.e.,

$$J_\mu = \sum_{i=1}^{4} \mu_{T_i}, \quad \text{with} \quad \mu_{T_i} = \sqrt{\frac{F_{x_i}^2 + F_{y_i^2}}{F z_i}}. \tag{14}$$

Many other objective function formulations (without any comparison of the performances) for CA can be found in the literature (e.g., in [3], [8], [11], and [37]), but this selection includes the most significant physical parameters that can be adopted and combined for CA design.

To facilitate a direct comparison of the results, the same set of inequality constraints has been imposed for each objective function. The evaluation of the objective functions is based on the following four criteria: 1) the smoothness (variation of the gradient) of the drivetrain torque profiles $T_i(a_y)$; 2) the uniformity of the longitudinal slip distribution among the four tires; 3) the sensitivity of $T_i(a_y)$ with the parameters of the electric drivetrain (such as the electric-motor drive efficiency map) and the tire–road friction coefficient; and 4) the energy efficiency of the resulting drivetrain actuation. Simulation results based on the reference understeer characteristics in Fig. 6 evaluated at $v = 90$ km/h and $a_x = 2.5$ m/s^2 are presented and discussed in detail.

Fig. 10 plots the drivetrain torque values at the wheels obtained with J_P and J_{SPL} as objective functions. In both cases, the target understeer characteristic has been defined by $K_U = 12$ deg/g, $a_y^* = 7$ m/s^2, and $a_{y,\,\max} = 8$ m/s^2, with the aim of increasing the cornering response of the baseline vehicle. Therefore, larger traction torque is required on the outer side of the corner (in this case, the right side of the vehicle) with respect to the inner side.

As shown in Fig. 10, the wheel torque values determined with J_P vary significantly when the lateral acceleration of the vehicle is between 4 and 6 m/s^2. This is due to the shape of the electric-motor efficiency maps. Below this range of a_y values, the corrective yaw moment is primarily generated at the rear axle through $T_{\mathrm{Right},\,R}$–$T_{\mathrm{Left},\,R}$. At about 4 m/s^2, the torque difference at the rear begins to reduce with rising a_y, which is compensated by a torque difference created at the front axle. At about 6 m/s^2, $T_{\mathrm{Right},\,R}$–$T_{\mathrm{Left},\,R} \approx 0$, and the entire yaw moment is generated at the front axle. At greater a_y values, $T_{\mathrm{Right},\,R}$–$T_{\mathrm{Left},\,R}$ increases again. The observed variation of the wheel torque distribution for steady-state conditions will impact the driving comfort during actual maneuvers in the time domain. Thus, the CA strategy based on J_P can be perceived negatively by the driver and the passengers. The rate of change of the wheel torque values can be reduced with proper constraints implemented in the online CA algorithm; however, such a reduction may affect the vehicle responsiveness to fast steering inputs. In contrast, with J_{SPL} the trends of the wheel torque values against a_y curves are smooth as this objective function is not related to the drivetrain efficiency maps, and the yaw moment contributions generated by the front and rear axles are very similar.

The same conclusions can be drawn when the wheel torque values evaluated with J_P are compared with those obtained with J_μ (see Fig. 11) and with J_{STD} (results omitted for brevity). Moreover, it was found that the results provided by J_{STD} and J_{SPL} are usually very similar.

The effectiveness of the slip-based CA objective functions is confirmed in Fig. 12, where the average slip of the four wheels and the standard deviation (plotted in the form of error bars) of the longitudinal slips with respect to their mean value (among the four tires) are compared for J_P and J_{SPL}. The trend of the mean value of the longitudinal slip as a function of a_y is nonlinear even at values of a_y where the understeer characteristic is still linear. This behavior can be ascribed to the nonlinear relationship between longitudinal and lateral tire forces. The mean value of the longitudinal slip remains nearly unaffected (up to a_y values close to the friction limits) by the particular CA objective functions, whereas its standard deviation is lower with the slip-based functions such as J_{SPL} (see Fig. 12). For the investigated operating conditions and vehicle parameters, the standard deviation with J_{SPL} is about half of the value obtained with J_P for most of the range of a_y. This reduction is

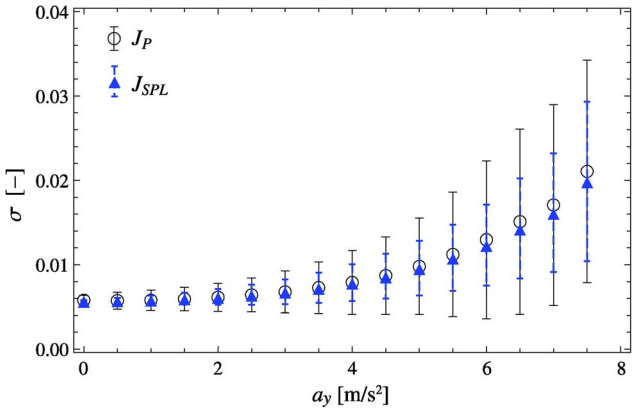

Fig. 12. Average longitudinal tire slip ratio of the four wheels and standard deviation for the TV vehicle with the understeer characteristic in Fig. 6 at $v = 90$ km/h and $a_x = 2.5$ m/s^2, considering J_P (minimum input power) and J_{SPL} (minimum longitudinal slip loss).

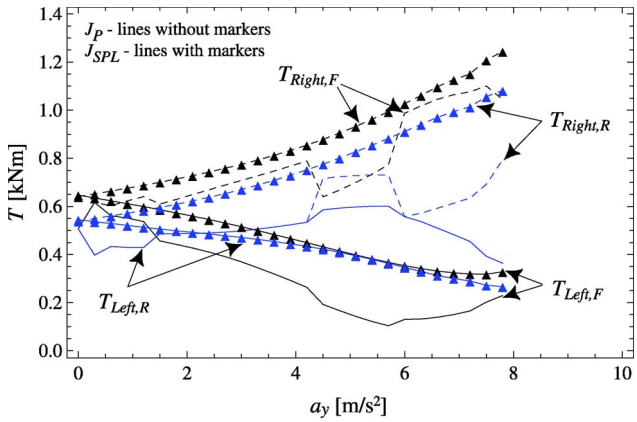

Fig. 14. Drivetrain torque values for the TV vehicle with the understeer characteristic in Fig. 6 at $v = 90$ km/h and $a_x = 2.5$ m/s^2 for J_P (lines without markers) and J_{SPL} (lines marked with markers). The simulations consider permanent-magnet motors.

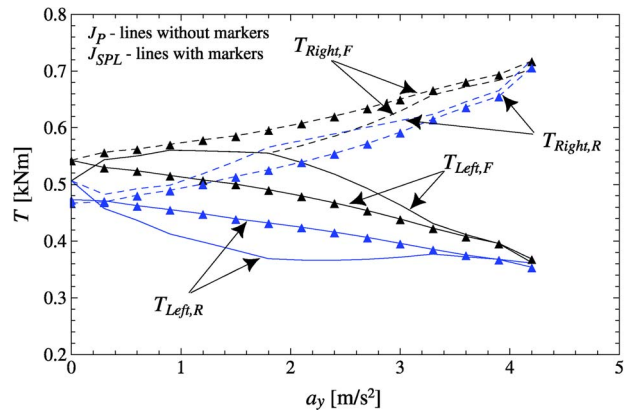

Fig. 13. Drivetrain torque values for the TV vehicle at $v = 90$ km/h and $a_x = 2.5$ m/s^2 ($K_U = 12$ deg/g; $\mu = 0.6$) for J_P (lines without markers) and J_{SPL} (lines with markers).

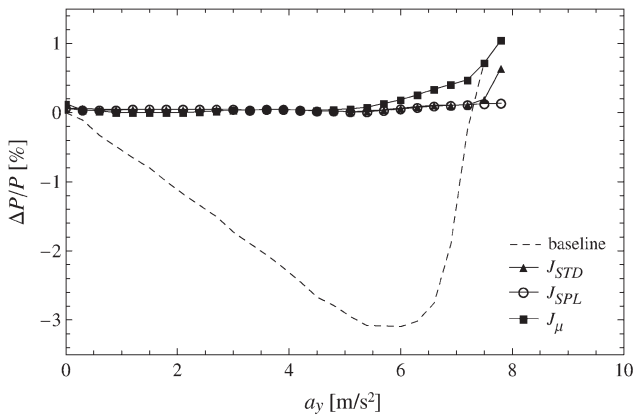

Fig. 15. Percentage difference of the input motor power for the objective functions J_{STD}, J_{SPL}, and J_μ for the vehicle with TV at $v = 90$ km/h and $a_x = 2.5$ m/s^2, with $K_U = 12$ deg/g and $\mu = 1$, and the vehicle without TV control ("baseline").

beneficial in terms of secondary phenomena such as tire wear. More importantly, the uniform distribution of slip ratios implies a greater margin before critical driving conditions are reached, which require the intervention of the traction control or antilock braking system. During these situations, the tracking capability of the reference yaw moment can be temporarily compromised. Hence, J_{SPL} can be assumed to enhance vehicle safety.

Owing to the linear relationship between longitudinal tire force and slip ratio σ for small values of σ, the same trend and magnitude of the slip variance among the four tires have been observed at small to medium values of a_y with J_μ and J_{SPL}. At a_y values close to $a_{y,\max}$, the magnitude of the wheel-slip variance is larger for J_μ than for J_{SPL}. This difference results from the nonlinearity of the tire characteristics. On a real vehicle application, J_μ could be preferred to J_{SPL} for practical reasons, such as simplicity of implementation.

Similar observations can be made in low friction conditions, as shown in Fig. 13 ($\mu = 0.6$), confirming the advantage achieved with slip-based strategies.

All the simulation results presented (see Figs. 10–13) were obtained with the same electric drivetrain characteristics. They are based on the switched reluctance electric motors that are implemented and tested within the European Union Seventh Framework Programme E-VECTOORC project [38]. As the efficiency maps of electric-motor drives may considerably vary, their influence was assessed by repeating the simulations with the alternative objective functions with a different electric-motor characteristic. In particular, a permanent-magnet dc motor for automotive traction with approximately the same peak power and torque values as the switched reluctance units was used. Fig. 14 shows the wheel torque distributions for J_P and J_{SPL} for this alternative powertrain hardware. With respect to J_P, the trend of the wheel torque values is not only different from the one presented in Fig. 10 but is also irregular. In terms of J_{SPL}, the simulation results show similar smooth trends and can be thus assumed to be nearly independent of the electric-motor drive characteristics.

To evaluate the influence of the CA objective functions on vehicle energy demand, the percentage difference $\Delta P/P$ of the overall motor input power for the strategies based on (12)–(14) with respect to the input power for J_P are compared in Figs. 15–17. Moreover, the figures show $\Delta P/P$ for the baseline vehicle, i.e., without actuation of the TV differential and an even torque distribution between the two electric-motor drives. Compared with J_P, the input power values to the electric

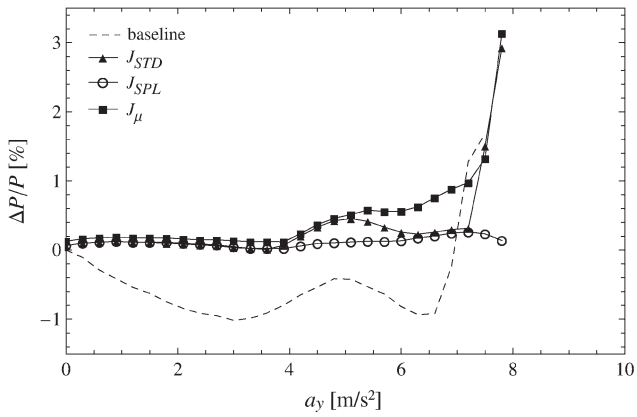

Fig. 16. Percentage difference of the input motor power for the objective functions $J_{\rm STD}$, $J_{\rm SPL}$, and J_μ for the vehicle with TV at $v = 90$ km/h and $a_x = 2.5$ m/s^2, with $K_U = 28$ deg/g and $\mu = 1$, and the vehicle without TV control ("baseline").

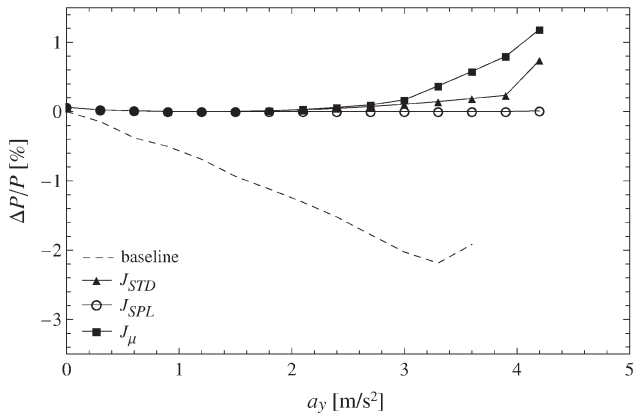

Fig. 17. Percentage difference of the input motor power for the objective functions $J_{\rm STD}$, $J_{\rm SPL}$, and J_μ for the vehicle with TV at $v = 90$ km/h and $a_x = 2.5$ m/s^2, with $K_U = 12$ deg/g and $\mu = 0.6$, and the vehicle without TV control ("baseline").

drivetrain required with the $J_{\rm STD}$ and $J_{\rm SPL}$ strategies are very similar. With the J_μ strategy, a slight input power increase at high a_y values can be observed. These findings hold true for very different control targets (i.e., $K_U = 28$ deg/g in Fig. 16) or low friction conditions (i.e., $\mu = 0.6$ in Fig. 17).

Moreover, the adoption of a TV system increases the input motor power demand by up to about 3%, compared with the baseline vehicle (see Figs. 15–17). The increase is caused by power losses associated with the actuation of the differential clutches required to generate the torque bias on each axle. As a consequence, a 4WD vehicle layout without TV differentials, i.e., with four individually controlled electric-motor drives, could be a more energy-efficient implementation of a TV system. Interestingly, the simulation results show that J_P allows reduction of the power losses in the TV differentials by about 8% relative to the other investigated objective functions.

V. Conclusion

A procedure for the offline design and evaluation of alternative TV controllers for fully electric vehicles has been presented. The results, which are obtained for a vehicle with central motors and TV differentials, demonstrate the effectiveness of TV control in tuning vehicle response. This is achieved through a set of reference understeer characteristics in conditions of constant and variable vehicle velocities. For actual implementation of a TV control system, the offline procedure allows the evaluation of the feedforward map of the control yaw moment, as a function of measured and estimated quantities, for a given set of vehicle and tire parameters.

The analysis of the CA criteria shows that energy-based cost functions provide marginal benefit in the selection of the individual wheel torque distribution. In contrast, objective functions based on tire slip distribution allow a smooth variation of the wheel torque values for all achievable lateral accelerations and yield only a marginal energy consumption penalty.

Similar analyses will be conducted in future studies for different multiple-motor vehicle layouts, including a detailed discussion of the regenerative and friction brake torque distributions during braking-while-cornering maneuvers.

References

[1] J. Kang, J. Yoo, and K. Yi, "Driving control algorithm for maneuverability, lateral stability, and rollover prevention of 4WD electric vehicles with independently driven front and rear wheels," *IEEE Trans. Veh. Technol.*, vol. 60, no. 7, pp. 2987–3001, Sep. 2011.

[2] K. Nam, H. Fujimoto, and Y. Hori, "Lateral stability control of in-wheel motor-driven electric vehicles based on sideslip angle estimation using lateral tire force sensors," *IEEE Trans. Veh. Technol.*, vol. 61, no. 5, pp. 1972–1985, Jun. 2012.

[3] M. Jonasson, J. Andreasson, S. Solyom, B. Jacobson, and A. S. Trigell, "Utilization of actuators to improve vehicle stability at the limit: From hydraulic brakes toward electric propulsion," *Trans. ASME, J. Dyn. Syst. Meas. Control*, vol. 133, no. 5, pp. 051003-1–051003-10, Jul. 2011.

[4] L. De Novellis, A. Sorniotti, and P. Gruber, "Optimal wheel torque distribution for a four-wheel-drive fully electric vehicle," *SAE Int. J. Passenger Cars–Mech. Syst.*, vol. 6, no. 1, pp. 128–136, May 2013.

[5] H. E. Tseng, B. Ashrafi, D. Madau, T. A. Brown, and D. Recker, "The development of vehicle stability control at Ford," *IEEE/ASME Trans. Mechatronics*, vol. 4, no. 3, pp. 223–234, Sep. 1999.

[6] M. Doumiati, A. C. Victorino, A. Charara, and D. Lechner, "Onboard real-time estimation of vehicle lateral tire-road forces and sideslip angle," *IEEE/ASME Trans. Mechatronics*, vol. 16, no. 4, pp. 601–614, Aug. 2011.

[7] L. Xiong and Z. Yu, "Control allocation of vehicle dynamics control for a 4 in-wheel motored EV," in *Proc. PEITS*, Shenzhen, China, Dec. 19–20, 2009, pp. 307–311.

[8] J. Wang and R. G. Longoria, "Coordinated and reconfigurable vehicle dynamics control," *IEEE Trans. Control Syst. Technol.*, vol. 17, no. 3, pp. 723–732, May 2009.

[9] D. Akaho, M. Nakatsu, E. Katsuyama, K. Takakuwa, and K. Yoshizue, "Development of vehicle dynamics control systems for in-wheel motor drive unit," presented at the JSAE Annual Congress, Yokohama, Japan, May 19–21, 2010, Paper 2010-5533.

[10] B. Tabbache, A. Kheloui, and M. Benbouzid, "An adaptive electric differential for electric vehicles motion stabilization," *IEEE Trans. Veh. Technol.*, vol. 60, no. 1, pp. 104–110, Jan. 2011.

[11] Y. Chen and J. Wang, "Design and experimental evaluations on energy efficient control allocation methods for overactuated electric vehicles: Longitudinal motion case," *IEEE/ASME Trans. Mechatronics*, in press.

[12] M. Canale, L. Fagiano, A. Ferrara, and C. Vecchio, "Vehicle Yaw control via second-order sliding-mode technique," *IEEE Trans. Ind. Electron.*, vol. 55, no. 11, pp. 3908–3916, Nov. 2008.

[13] M. Canale, L. Fagiano, A. Ferrara, and C. Vecchio, "Comparing internal model control and sliding-mode," *IEEE Trans. Intell. Transp. Syst.*, vol. 10, no. 1, pp. 31–41, Mar. 2009.

[14] A. van Zanten, "Bosch ESP Systems: 5 Years of Experience," presented at the Society Automotive Engineers World Congr., Detroit, MI, USA, 2000, SAE Paper 2000-01-1633.

[15] S. Chang and T. Gordon, "Model-based predictive control of vehicle dynamics," *Int. J. Veh. Autonom. Syst.*, vol. 5, no. 1/2, pp. 3–27, Sep. 2007.

[16] G. Yin, N. Chen, and P. Li, "Improving handling stability performance of four-wheel steering vehicle via μ-synthesis robust control," *IEEE Trans. Veh. Technol.*, vol. 56, no. 5, pp. 2432–2439, Sep. 2007.
[17] S. Tanaka, M. Kawamoto, and H. Inagaki, "Regenerative braking electric vehicle with four motors," U.S. Patent 5 148 883, Sep. 22, 1992.
[18] N. Mutoh, "Driving and braking torque distribution methods for front- and rear-wheel-independent drive-type electric vehicles on roads with low friction coefficient," *IEEE Trans. Ind. Electron.*, vol. 59, no. 10, pp. 3919–3933, Oct. 2012.
[19] S. Yim, J. Choi, and K. Yi, "Coordinated control of hybrid 4WD vehicles for enhanced maneuverability and lateral stability," *IEEE Trans. Veh. Technol.*, vol. 61, no. 4, pp. 1946–1950, May 2012.
[20] S. Fallah, A. Khajepour, B. Fidan, S. K. Chen, and B. Litkouhi, "Vehicle optimal torque vectoring using state-derivative feedback and linear matrix inequality," *IEEE Trans. Veh. Technol.*, vol. 62, no. 4, pp. 1540–1552, May 2013.
[21] J. Tjonnas and T. A. Johansen, "Stabilization of automotive vehicles using active steering and adaptive brake control allocation," *IEEE Trans. Control Syst. Technol.*, vol. 18, no. 3, pp. 545–558, May 2010.
[22] M. Naraghi, A. Roshanbin, and A. Tavasoli, "Vehicle stability enhancement—An adaptive optimal approach to the distribution of tyre forces," *Proc. IMechE D, J. Autom. Eng.*, vol. 224, no. 4, pp. 443–453, Apr. 2010.
[23] H. B. Pacejka, *Tyre and Vehicle Dynamics,* 2nd ed. Oxford, U.K.: Butterworth-Heinemann, 2006.
[24] D. A. Crolla and D. Cao, "The impact of hybrid and electric powertrains on vehicle dynamics, control systems and energy recuperation," *Veh. Syst. Dyn.*, vol. 50, no. S1, pp. 95–109, Jan. 2012.
[25] T. D. Gillespie, *Fundamentals of Vehicle Dynamics*. Warrendale, PA, USA: SAE Int., 1992.
[26] J. Reimpell, H. Stoll, and J. Betzler, *The Automotive Chassis: Engineering Principles,* 2nd ed. Oxford, U.K.: Butterworth-Heinemann, 2001.
[27] W. F. Milliken and D. L. Milliken, *Chassis Design–Principles and Analysis*. Warrendale, PA, USA: SAE Int., 2002.
[28] F. Cheli, L. Kakalis, and A. Zorzutti, "A torque vectoring control logic for active high performance vehicle handling improvement," in *Proc. ASME IDETC/CIE*, Las Vegas, NV, USA, Sep. 4–7, 2007, pp. 1223–1232.
[29] W. F. Milliken and D. L. Milliken, *Race Car Vehicle Dynamics*. Warrendale, PA, USA: SAE Int., 1995.
[30] M. Abe, "A theoretical analysis on vehicle cornering behaviors in acceleration and in braking," *Veh. Syst. Dyn.*, vol. 15, no. S1, pp. 1–14, Jan. 1986.
[31] Y. Shibahata, K. Shimada, and T. Tomari, "Improvement of vehicle maneuverability by direct Yaw moment control," *Veh. Syst. Dyn.*, vol. 22, no. 5/6, pp. 465–481, Jan. 1993.
[32] *Road Vehicles—Vehicle Dynamics and Road-Holding Ability—Vocabulary*, ISO Std. 8855:2001, 2001.
[33] K. Sawase, Y. Ushiroda, and T. Miura, "Left-right torque vectoring technology as the core of Super All Wheel Control (S-AWC)," *Mitsubishi Motors Tech. Rev.*, no. 18, pp. 16–23, 2006.
[34] L. Gao, "Dynamic lithium-ion battery model for system simulation," *IEEE Trans. Compon. Packag. Technol.*, vol. 25, no. 3, pp. 495–505, Sep. 2002.
[35] R. H. Byrd, M. E. Hribar, and J. Nocedal, "An interior point algorithm for large-scale nonlinear programming," *SIAM J. Opt.*, vol. 9, no. 4, pp. 877–900, 1999.
[36] N. Amann, J. Bocker, and F. Prenner, "Active damping of drive train oscillations for an electrically driven vehicle," *IEEE/ASME Trans. Mechatronics*, vol. 9, no. 4, pp. 697–700, Dec. 2004.
[37] M. Gerard and M. Verhaegen, "Global and local chassis control based on load sensing," in *Proc. Amer. Control Conf.*, St. Louis, MO, USA, Jul. 10–12, 2009, pp. 677–682.
[38] E-VECTOORC FP7 Project. [Online]. Available: http://www.e-vectoorc.eu/

Leonardo De Novellis (M'12) received the M.Sc. degree in mechanical engineering and the Ph.D. degree in mechanical and biomechanical design from the Polytechnic University of Bari, Bari, Italy, in 2006 and 2010, respectively.

Since 2011, he has been a Research Fellow with the University of Surrey, Guildford, U.K. His main research interests include continuously variable transmissions and vehicle dynamics.

Aldo Sorniotti (M'12) received the M.Sc. degree in mechanical engineering and the Ph.D. degree in applied mechanics from the Polytechnic University of Turin, Turin, Italy, in 2001 and 2005, respectively.

He is a Senior Lecturer of advanced vehicle engineering with the University of Surrey, Guildford, U.K. He is the Project Coordinator of the Electric Vehicle Control of Individual Wheel Torque for On- and Off-Road Conditions (E-VECTOORC) Project. His main research interests include vehicle dynamics control and automotive transmissions for electric vehicles.

Patrick Gruber received the M.Sc. degree in motorsport engineering and management from Cranfield University, Cranfield, U.K., in 2005 and the Ph.D. degree in mechanical engineering from the University of Surrey, Guildford, U.K., in 2009.

Since 2009, he has been a Lecturer of advanced vehicle systems engineering with the University of Surrey. His current research interests include tire dynamics and development of novel tire models.